NASA Technical Memorandum 104626

Elastic Moduli and Damping of Vibrational Modes of Aluminum/Silicon Carbide Composite Beams

Henning Leidecker

March 1996

NASA Technical Memorandum 104626

Elastic Moduli and Damping of Vibrational Modes of Aluminum/Silicon Carbide Composite Beams

Henning Leidecker
Goddard Space Flight Center
Greenbelt, Maryland

National Aeronautics and
Space Administration

Goddard Space Flight Center
Greenbelt, Maryland

1996

This publication is available from the NASA Center for AeroSpace Information,
800 Elkridge Landing Road, Linthicum Heights, MD 21090-2934, (301) 621-0390.

Abstract

Elastic and shear moduli were determined for two aluminum matrix composites containing 20 and 40 volume percent discontinuous silicon carbide, respectively, using transverse, longitudinal, and torsional vibrational modes of specimens prepared as thin beams. These moduli are consistent with those determined from stress-strain measurements. The damping factors for these modes were also determined. Thermal properties are used to show that part of the damping of transverse modes is caused by the transverse thermal currents discussed by C. Zener (*thermoelastic damping*); this damping is frequency-dependent with a maximum damping factor of ~ 0.002. The remaining damping is frequency-independent, and has roughly similar values in transverse, longitudinal, and torsional modes: $\sim 0.000\,1$.

Contents

List of Tables

List of Figures

Chapter 1

Introduction

The stresses occurring during the launch of a spacecraft excite vibrational modes in both the spacecraft and the payload. It is common experience that the damping factors of these modes[1] are in the range $g \approx 0.01$ to 0.1 ; see References [6, 12]. These damping values arise from energy losses in joints, from devices explicitly introduced to absorb vibrational energy (dampers), from coupling with air, and from losses within the materials themselves (material damping). These values are chosen to fit observations of the vibration modes; they are not the results of calculations based upon reliable models of joints and other interconnections, reliable models of air interactions, and basic material properties of the parts of the craft. Hence, there is some vagueness as to what fraction each of these mechanisms contributes to the observed damping values, but it is generally accepted that most of this damping is caused by energy dissipation in dampers and in joints, with some small losses into the air; energy losses within the materials account for very little of the total. Hence, the study of material damping has been of little importance for the understanding of and control of vibrations occurring during launches.

Vibrational behaviors during standard operations in orbit are quite different from those at launch: there is no air damping, and operational activities produce small stresses which do not induce joint-slippage, and sometimes even fail to excite dampers (i.e., the joints and sometimes the dampers exhibit *stiction*, becoming rigid at small applied stresses). A general estimate is that damping factors are roughly 10 times smaller during orbital operations.[2] Hence, material damping can become a substantial part of the total damping.

Modes with $g \approx 0.01$ cause enough motion in Landsat-4 to compromise pointing accuracy [18]. Vibrations are expected to be an increasingly serious problem, since pointing accuracy requirements are increasing. One approach to the control of orbital vibrations involves a study of the amount of material damping that is passively available from the structure itself. Other approaches use dampers and active servocontrol systems, but even then, a complete analysis requires knowledge of the material damping values.

There have been studies of material damping at GSFC [4, 2] and elsewhere [25, 3, 20, 24]. These have concluded that the damping factor for the flexural modes of metal beams is well-described by a mechanism elucidated by Clarence Zener in 1948, [25]: *Zener thermoelastic damping* operates

[1] A glossary of measures of damping is in Appendix B. The damping factor g is used in this report.

[2] Private communication from Mr. J. Sudey, formerly of Code 716.2 at GSFC. He is the coauthor of Reference [18].

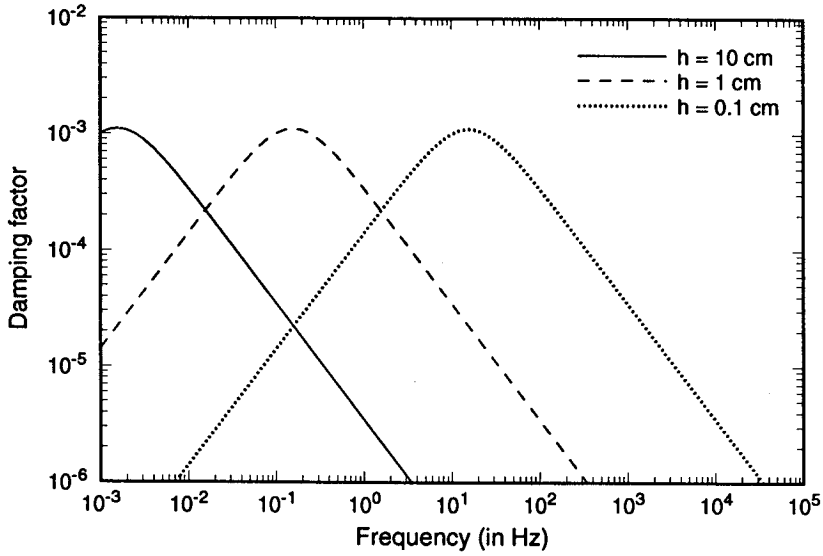

Figure 1.1: The damping factor for flexural vibrations of rectangular beams (thickness $\ll$ width) of 6061-T6 aluminum versus frequency. These curves are based upon the equations in Appendix C and standard values for the thermoelastic parameters.

in flexural modes, but not in extensional[3] or torsional modes; it is a function of frequency, and achieves a maximum value at a *Zener frequency* f_{Zener} which is proportional to the reciprocal of the square of the thickness of the beam, h: $f_{\text{Zener}} \propto 1/h^2$. As the frequency of a vibrational mode departs from the Zener frequency, its damping decreases strongly until other damping mechanisms mask it. If the frequency range of a flexural mode is within an order of magnitude of the Zener frequency, then Zener damping is likely to dominate.

For standard aluminum alloys, the maximum Zener damping is $g_{\text{Max}} \approx 0.002$, and this occurs at $f_{\text{Zener}} \approx 20$ Hz for beams or sheets that are 2 mm thick: see Figure 1.1 for the frequency dependence of Zener damping for the three thicknesses 0.1 cm, 1.0 cm, and 10 cm.

Hence, Zener damping is important over a range of frequencies of significance to many spacecraft operations. Using frequencies both lower[4] and higher than the Zener frequency, we have measured transverse mode damping factors in the lab as small as $g \approx 3 \times 10^{-5}$ for aluminum alloys. Longitudinal and torsional modes are not affected by Zener damping; laboratory measured values range from 10^{-3} to 10^{-4}. These measurements imply that it is not safe to assume that the values observed in Landsat-4 operations are the smallest possible.

Addition of silicon carbide (SiC) to aluminum (Al), either as whiskers (SiC_W) or as a fine particulate (SiC_P), increases the moduli and ultimate strength faster than the density and decreases the thermal expansion [14]. Hence, Al+SiC composites have a use in areas in which high strength, low weight, and low thermal expansion — relative to standard aluminum alloys — are desired. It is necessary to measure the damping of this material to complete the characterization necessary for its use in spacecraft, whether passive or active damping systems are to be used.

[3]Strictly speaking, extensional (i.e., longitudinal) modes exhibit Zener thermoelastic damping but f_{Zener} is so low that this damping is not observable in current practice.

[4]Tip-weighted cantilever beams were used; details will be reported separately.

We have studied the vibrational behaviors of beams of Al+SiC over a range of frequencies from 60 Hz to 30 000 Hz, have confirmed existing values for the elastic moduli of these materials, and have observed damping factors for Al, for Al with 20% SiC whiskers,[5] and for Al with 40% SiC particles (1–5 μm nominal diameter). Our results are restricted to strains of 10^{-3} or less, which is appropriate for many orbital operations, though not for launch. We observed no strain dependence in either the modulus or the damping within this range, but an increase in damping is expected for larger strains [4]. Modeling thermal deformations requires the coefficients of thermal expansion and of thermal conductivity; we report values for these quantities and use them to show that Zener damping dominates the damping of the flexural modes of beams of these materials as long as the vibration frequency is within an order of magnitude of the Zener frequency. For more distant frequencies, another damping mechanism (or mechanisms) becomes visible, with a damping factor that is about the same in transverse, longitudinal, and torsional modes.

[5]Each concentration is measured using its *volume fraction*, often denoted by v/o, but denoted by $\mathcal{VF}$ here.

Chapter 2

Specimens

Standard 6061-T6 aluminum alloy was used as the base-line material. A test beam was fashioned from it, labeled CONTROL, and numbered #0.

ARCO[1] provided us with a specimen of 6061-T6 aluminum alloy with 20% silicon carbide in the form of whiskers: their designation is SXA 6061-T6/20% SiC_W; the material was manufactured in 1985. It was wire-cut at GSFC into two beams, one of which is considered in this report. The wire-cutting operation left a gray surface finish; also, the beam was bent into a slight arc. This specimen is labeled GRAY (#1).

General Electric Company[2] (GE) provided us with three specimens of 6061-T6 aluminum alloy with 40% silicon carbide in the form of roughly equiaxial particles of 1 μm to 5 μm diameter: we denote this material as Al+SiC_P. They obtained this material from ARCO in 1986. GE fashioned these into rectangular beams with the same lengths and widths, and with thicknesses decreasing in the ratios $1/\sqrt{10}$, which gives three well-spaced fundamental vibrational frequencies. These beams have bright, near mirror finishes, and are referred to as THICK (#2), MEDIUM (#3), and THIN (#4), respectively.

[1] ARCO Chemical Company, Advanced Material, Route 6, Box A, Greer, SC 29651.

[2] The specimens were provided in 1986 by the Space System Division, which was then at Valley Forge Space Center, P.O. BOX 8555, Philadelphia, PA 19101.

Chapter 3

Methodology and measurements

Most of the work involved in deforming a metal or a metal composite is stored as recoverable (i.e., elastic) energy. In the absence of joint friction and air friction, it is unusual to lose as much as 0.1% to damping, and losses of less than 1 part in 10^{-7} have been observed in specialized circumstances such as massive aluminum beams at a temperature of about 4 K. Hence, it can be difficult to measure the damping modulus in any experiment that involves a direct comparison with the elastic modulus. But relatively small damping implies that specimens can be excited into well-defined resonances. At each resonance, the elastic forces caused by deformation exactly balance the inertial forces caused by motion, leaving only the damping forces to balance the driving forces. By observing the outcome of the latter balance, the damping can be measured — this is the *driven resonance* method. Alternately, if the driving force is stopped so that the specimen is left in free (not forced) oscillation, then the damping forces slowly dissipate the elastically stored energy. By observing the rate of this dissipation, the damping can be measured — this is the *free decay* method. As a bonus, the elastic modulus can be calculated from the frequency of oscillation.

The main drawback of either method is that the damping force can be measured only at each of the resonant frequencies of the specimen. It is as if the spectrum of resonant frequencies used in a given experiment is a set of narrow "viewing windows" into the complete frequency dependence of the damping force. This drawback can be overcome when it is possible to interpolate the behavior between observed frequencies; hence, it is desirable to work with a set of specimens of the material of interest, shaping the specimens so that they have a wide range of overlapping resonant frequencies.

A material has a distinct elastic modulus for each distinct mode of deformation. For example, the *bulk modulus* controls changes in volume that do not change the shape of an element. For an isotropic material, all moduli can be related to two moduli which we shall choose as the Young's modulus E and the shear modulus G. Correspondingly, a material has distinct types of damping, one for each distinct mode of deformation. For example, it is well-known from ultrasonic absorption studies that the damping of shear waves is different from the damping of longitudinal waves. We must expect that, in general, the damping of the longitudinal modes of a beam is different from the damping of the transverse and the torsional modes.

In summary, we fashion the materials of interest into beams of uniform cross section and study both their driven and their free resonances in order to determine the set of elastic moduli and the damping factors for various deformation modes of the material.

3.1 The dimensions, densities, and void contents of the specimens

A metal matrix composite is characterized by both the volume fraction ($\mathcal{VF}$) of the reinforcing material and by the volume fraction of voids that invariably result from current manufacturing techniques. As little as 2% voids can cut in half the ultimate strength of an Al+30% SiC composite [13]. The effect of voids upon the moduli is much smaller: the relative decrease is roughly the void fraction. If the amounts of matrix and reinforcement are known, either from the manufacturing conditions or from an analysis, then the void content can be determined from measurements of the density [13]:

$$\mathcal{VF}_{\text{voids}} = 1 - \left[\frac{\rho_{\text{specimen}} - (\rho_{\text{SiC}} - \rho_{\text{Al}}) \cdot \mathcal{VF}_{\text{SiC}}}{\rho_{\text{Al}}}\right]. \tag{3.1}$$

The standard technique for precise density determination involves weighings in air and in a liquid. However, these specimens were accurately machined to be rectangular beams, which allowed accurate determination of their volumes from their dimensions. The width and thickness of each specimen were measured at thirty positions with a micrometer, and the lengths were measured with a traveling microscope. Each beam was weighed on each of three laboratory balances. The dimensions, the masses, and the computed densities are listed in Table 3.1.

Table 3.1: Measured Masses and Dimensions, and Computed Densities

	CONTROL beam (#0)	GRAY beam (#1)	THICK beam (#2)	MEDIUM beam (#3)	THIN beam (#4)
$\mathcal{VF}_{\text{SiC}}$	0% SiC	20% SiC	40% SiC		
mass (g)	13.931 5 ±0.004%	25.814 ±0.01%	69.427 9 ±0.000 60%	22.794 5 ±0.002 4%	7.410 9 ±0.003 9%
length (cm)	25.405 ±0.001%	30.45 ±0.10%	27.932 ±0.001%	27.932 ±0.001%	27.934 ±0.001%
width (cm)	1.272 ±0.03%	1.515 ±0.07%	1.269 2 ±0.024%	1.271 2 ±0.024%	1.270 2 ±0.024%
thickness (cm)	0.159 2 ±0.20%	0.199 ±0.5%	0.682 2 ±0.046%	0.223 3 ±0.13%	0.072 9 ±0.41%
density (g/cc)	2.708 ±0.3%	2.81 ±0.8%	2.871 ±0.072%	2.875 ±0.16%	2.866 ±0.43%

Density (weighted average, corrected to vacuum)	
0% SiC	(2.71 ± 0.01) g/cc
20% SiC_W	(2.81 ± 0.02) g/cc
40% SiC_P	(2.872 ± 0.002) g/cc

Solving Equation 3.1, using the standard values $\rho_{\text{Al}} = 2.71$ g/cc and $\rho_{\text{SiC}} = 3.21$ g/cc, gives

$$\begin{aligned} \text{Al+20\% SiC}_W\text{:} \quad & \mathcal{VF}_{\text{voids}} = (0 \pm 1)\% \\ \text{Al+40\% SiC}_P\text{:} \quad & \mathcal{VF}_{\text{voids}} = (1.4 \pm 0.2)\%. \end{aligned}$$

These results fall within the range expected for these materials.

3.2 Vibrational spectrum and moduli of beams

Formulas relating bending moduli to the vibrational spectrum of thin beams of circular or rectangular cross section were theoretically established and experimentally verified by the mid-1800's. Recommendations that the vibrational spectra be used to measure bending moduli date from the first studies in 1740 by L. Euler and D. Bernoulli. But it was not until about 1935 that this method began to be used in a routine manner [16]. For the beams used in practice, it is often necessary to introduce corrections to the classic results.[1] Reliable methods of doing this were suggested by Pickett in a painstaking review of relevant theory [11] and confirmed in a detailed series of experiments by a group led by Spinner [17, 15, 19]. These methods have achieved moduli accurate to within 0.01% under ideal circumstances; they are summarized in Reference [16], and in the related standard method C215-85 [1] of the American Society for Testing and Materials (ASTM). We used the procedures of Reference [16] to reduce our data.

A block diagram of the apparatus is given in Figure 3.1. Our specimens were fashioned into beams of rectangular cross section, and a small iron disk (mass per disk = 0.090 ± 0.001 g) was attached to each end. Each beam was electromagnetically excited at one end, and its motion was electromagnetically detected at the other end. The driving frequency was varied until a resonance frequency was excited. The position of the exciter/detector modules influenced the class of modes excited: transverse (i.e., flexural), longitudinal (i.e., extensional), or torsional modes. Each beam was suspended upon lightweight threads positioned at the n^{th} vibrational nodal lines, while the beam was driven at its n^{th} modal frequency. The loading effect of the iron disks was accounted for with the procedures of Reference [16]. (The THIN beam's frequencies required the largest corrections: 5%; these corrected frequencies are reliable to within 0.1%. The THICK beam's frequencies required the smallest corrections: 0.5%; these corrected frequencies are reliable to within 0.03%.) Frequencies were derived from a frequency generator with a range of 1 μHz to 20 MHz and a resolution and accuracy of 1 μHz below 100 kHz and 1 mHz above 100 kHz.

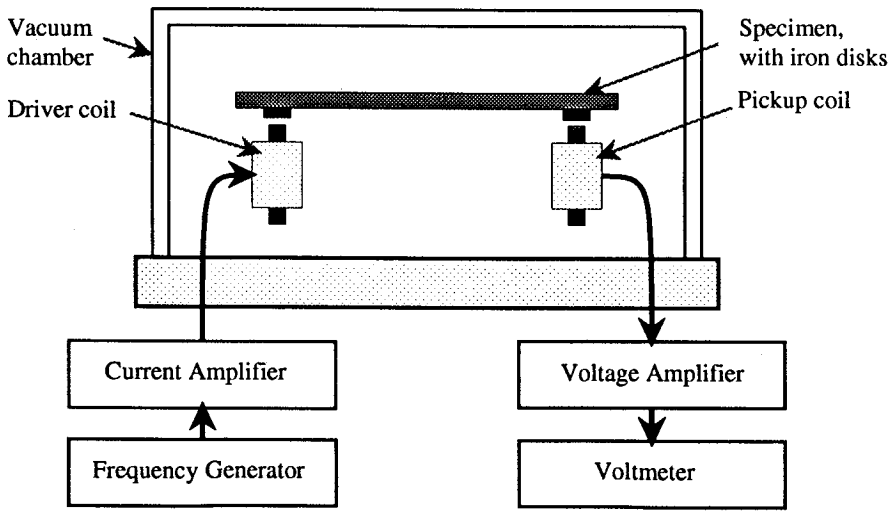

Figure 3.1: General diagram of the experimental apparatus.

[1] The necessary corrections are still not rigorously known: see Appendix A.

3.3 Damping measurements

There are a number of measures of damping in current use [25, 5, 8]. We will use the *damping factor* g; some others are defined in Appendix B. Vibrational damping was studied using two methods, *driven resonance* and *free decay.*

Driven resonance The beam was driven into resonance at its n^{th} mode and both the amplitude of its motion $\mathcal{A}$ and the frequency of this resonance f_n were recorded. Then the driving frequency was raised until the amplitude of response dropped to $\mathcal{A}/\Re$ where $\Re$ is a chosen constant such as 2, and this new frequency $f^+_{n,\Re}$ was recorded. Finally, the frequency was lowered below f_n until the amplitude again dropped to $\mathcal{A}/\Re$; this is $f^-_{n,\Re}$. The damping factor for this mode is

$$g_n = \frac{1}{\sqrt{\Re^2 - 1}} \left(\frac{f^+_{n,\Re} - f^-_{n,\Re}}{f_n} \right). \tag{3.2}$$

Our usual procedure was to use *half-amplitude* points ($\Re = 2$), and so

$$g_n = \frac{1}{\sqrt{3}} \left(\frac{f^+_{n,2} - f^-_{n,2}}{f_n} \right). \tag{3.3}$$

However, many workers use detectors that respond to the intensity of the vibration $\mathcal{A}^2$ (this is proportional to the power) and not its amplitude $\mathcal{A}$. For *half-power* points, $\Re = \sqrt{2}$, and

$$g_n = \frac{\left(f^+_{n,\sqrt{2}}\right) - \left(f^-_{n,\sqrt{2}}\right)}{f_n}. \tag{3.4}$$

We have found the choice $\Re = 2$ to be most convenient.

When measured in air, the resonant frequency of a given mode was typically stable to within 0.1% for times on the order of an hour, since the room temperature was typically stable to within about 0.5 ℃ during that time. However, promptly upon beginning a pump-down, the resonant frequency would begin to drop and not stabilize until after several hours. This effect is probably related to a temperature change of the beam. The frequency shift would often amount to a significant fraction of $f^+ - f^-$ in the time required to make a measurement; hence, corrections for these shifts were made and frequently checked against measurements made after equilibrium had again been established.

To test that the behavior of the beams we studied was linear, we repeatedly varied the driving force by factors of 10 to 100. We found no changes in either the resonant frequency or the damping factor. However, we did find a detectable decrease in the resonant frequency when the driving force was increased by more than 100 times the value usually used; this corresponded to strains of 0.003 or larger.

Free decay The frequency of the excitation was adjusted to produce a resonance at the n^{th} mode, and then the excitation was suddenly terminated. This frequency f_n and the time τ_n for the amplitude of the freely decaying oscillations to decrease by the fraction $1/e \approx 0.3679$ were observed. Then

$$g_n = 1/(\pi \tau_n f_n). \tag{3.5}$$

We frequently tested the time dependence of the decaying amplitude, always finding it to be an exponential decay from amplitudes corresponding to strains of roughly 0.002 to several orders of magnitude smaller; hence, the damping is accurately linear over this range of strains.

Comparison of methods We have found that detector noise and other experimental sources of errors affect the driven resonance and the free decay methods in opposite ways, so that agreement between them is evidence that these errors are unimportant and that the value of g_n is reliable. Initially, the results for driven resonance differed from the results for free decay by more than 50%, which forced a search for sources of errors. The major errors were a noisy voltage amplifier and incorrect zero positions in both the voltmeter (used in AC mode in the driven resonance measurement) and the pen recorder (used in AC mode in the free decay measurement). After eliminating errors, we obtained agreement to within about 3% to 10% for all the values of g_n reported here: we use 10% as the nominal value for the uncertainty in g.

Effect of the beam's suspension Several findings confirm that our method of suspension did not introduce detectable damping:

- The damping measured for aluminum containing no silicon carbide is in good agreement with Zener's thermoelastic model for damping factors as low as $g = 10^{-5}$; hence, damping due to the supports is less than 10^{-6}.
- In one series of studies, the threads were positioned at various distances from the calculated nodal positions. The damping increased quadratically with displacement from the nodal positions. The increase was insignificant whenever the threads were within about a millimeter of the calculated nodal lines. This criterion is easily met in practice. (See Figure 3.2.)

These studies were conducted both in air and in a vacuum of better than 10^{-6} torr. *Air damping* is a complicated phenomena; there is currently no adequate theory for rectangular beams vibrating in air. The safest course is to remove the air, rather than to attempt to correct for the damping caused by air.

Other methods Zener [25] studied reed specimens vibrating in a vacuum. Granick and Stern [4] determined the vibration amplitudes at the root of a center-driven cantilever and at its tips, and determined the damping factor from the ratio of these amplitudes, both in air and in a vacuum. (This is a version of the *magnification factor* method: see the definition of $Q_{\mathcal{M}}$ in Appendix B.) Professor Crawley and his students at the Massachusetts Institute of Technology have studied a freely vibrating beam in free-fall in a vacuum [3]. These beams were well decoupled from their environment except for attached strain gauges used to observe the vibrations, which did not introduce detectable damping, since the observed damping was noted to be independent of the number of strain gauges. Each of these workers has also studied the transverse modes of standard aluminum and has found it to be described by Zener thermoelastic damping.

Data The observed frequencies and observed damping factors of the various specimens are listed in Tables 3.2, 3.3, and 3.4. The accuracy of the frequency values is about ± 0.3 in the last digit

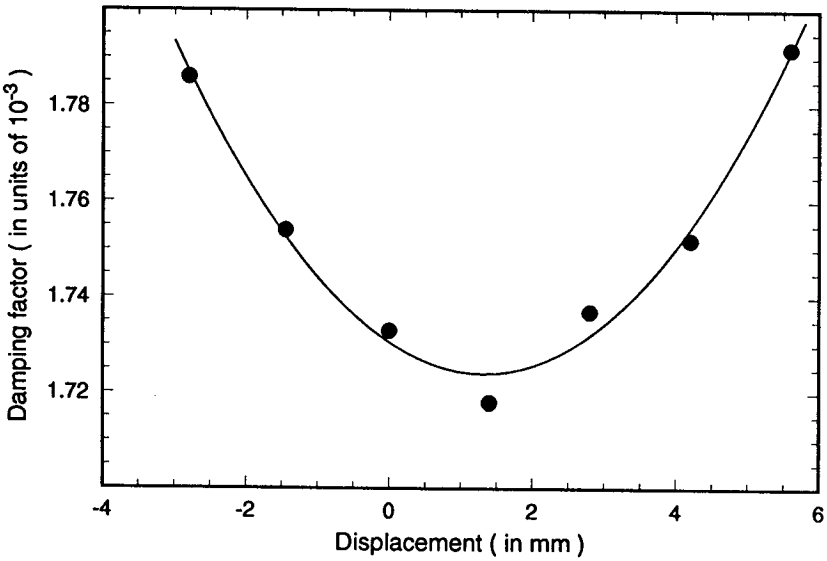

Figure 3.2: The observed damping factor versus the displacement of the support threads from the nodal positions computed using uniform beam theory for the THIN beam vibrating in air in its fundamental mode. The minimum is at a displacement of +1.33 mm from the computed nodal lines, in the direction of the iron disks: this is the shift in the nodal lines expected because of the mass loading of these disks. Note that the scatter in the damping factor is roughly ±0.3% for this set of measurements.

quoted. The accuracy of the damping factor values is roughly ±3%. All measurements were made at room temperature: (22 ± 2) ℃.

Table 3.2: Measured Longitudinal Frequencies and Dampings for the THICK Specimen

Beam	Vibrational mode number, n	Observed frequency, $f_{n,\mathrm{obs}}$ (Hz)	Observed damping factor, $g_{n,\mathrm{obs}}$ (units of 10^{-4})
THICK (#1)	1	12 906.0	0.462
	2	25 783.4	0.651
	3	38 650.8	0.532

Table 3.3: Measured Torsional Frequencies and Dampings for the MEDIUM and THICK Specimens

Beam	Vibrational mode number, n	Observed frequency, $f_{n,\text{obs}}$ (Hz)	Observed damping factor, $g_{n,\text{obs}}$ (units of 10^{-4})
THICK (#2)	1	6 057.39	2.28
	2	12 090.50	1.67
	3	18 124.46	2.36
MEDIUM (#3)	1	2 537.40	1.39
	2	5 052.04	1.57
	3	7 579.86	4.75

Table 3.4: Measured Transverse Frequencies and Dampings for the Specimens

Beam	Vibrational mode number n	Observed frequency $f_{n,\text{obs}}$ (Hz)	Observed damping factor $g_{n,\text{obs}}$ (units of 10^{-4})
CONTROL (#0)	1	124.7	14.9
	2	343.8	5.95
	3	673.5	3.10
GRAY (#1)	1	132.4	10.5
	2	384.4	3.4
	3	762.7	2.2
THICK (#2)	1	645.34	1.32
	2	1 770.84	0.96
	3	3 450.7	1.16
	4	5 661.2	⋆
MEDIUM (#3)	1	209.50	3.65
	2	577.37	2.24
	3	1 130.85	1.43
	4	1 870.0	1.03
	5	2 793.7	0.86
THIN (#4)	1	64.9	19.3
	2	184.9	15.5
	3	363.3	12.0
	4	602.4	8.73
	5	902.7	6.71
	6	1 264.7	5.11
	7	1 683.4	⋆
	8	2 167.0	⋆
	9	2 711	⋆
	10	3 313	⋆

Note: Cases for which there are no measurements are marked with a star (⋆).

Chapter 4

Material properties

Zener's theory of thermoelastic damping predicts a damping factor that depends completely upon the Young's modulus E and certain thermal properties: the linear thermal expansion $\alpha = d \ln \ell / dT$ where ℓ is a linear dimension of the specimen such as its length, the volume specific heat c, and the thermal diffusivity $\kappa_{td} = k_T / c$ where k_T is the thermal conductivity. (See Appendix C.) The volume specific heat c is computed from the more commonly tabled mass specific heat $c^{[m]}$ using $c = \rho c^{[m]}$ where ρ is the density. Values for all of the required properties are in Reference [14]; however, the scatter in the reported values for α and especially κ_{td} is large, probably because commercial processing was still variable when the data used in Reference [14] were being taken ($\sim$ 1975–1982). GE provided us with values for α, the mass specific heat $c^{[m]}$, and κ_{td} for the specimens they sent us. We also measured α for both the 20% SiC_W and the 40% SiC_P specimens. These data are plotted in Figures 4.1 through 4.3.

The values for Young's modulus are shown in Figure 5.1 in the next chapter, along with the results obtained from the vibrational spectra of the specimens reported here.

There is no completely reliable model for computing the thermal expansion of these composites from the values of the component materials, and so we must rely on the data alone. We have the following at 22 ℃. For 0% SiC content, $\alpha_{0\%} = (23.2 \pm 0.5) \times 10^{-6}/$ ℃ for both pure aluminum and 6061 alloy. For 20% SiC content, all three data sets (those from GSFC, from GE, and from Reference [14]) are in agreement to within their respective uncertainties; the weighted average is $\alpha_{20\%} = (14.0 \pm 0.9) \times 10^{-6}/$ ℃. For 40% SiC content, the GSFC data is in good agreement with that of Reference [14]; the GE value is higher than these other values, but not by more than its quoted uncertainty: the weighted average is $\alpha_{40\%} = (12.5 \pm 0.8) \times 10^{-6}/$ ℃.

The thermal expansion of pure aluminum and of 6061 alloy increases noticeably over the temperature range shown in Figure 4.1; however, no increase is observable for 20% or 40% SiC content for the GSFC data or for 40% SiC content for the data from Reference [14]. Indeed, the data from Reference [14] indicate a decrease in the thermal expansion of 20% SiC content material. More work is needed here.

The mass specific heat can be calculated from the rule of simple mixing, since there are no chemical interactions between the aluminum and the silicon carbide: this rule is usually reliable to within

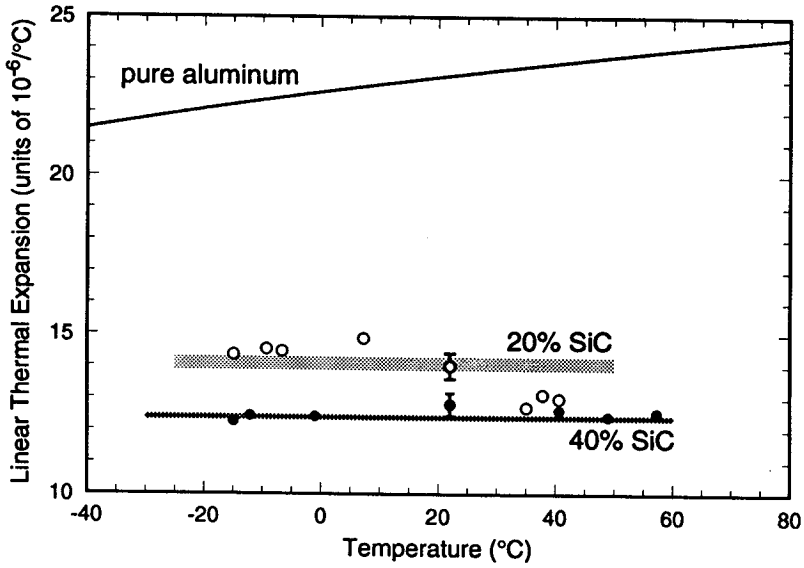

Figure 4.1: The thermal expansion of Al+SiC versus temperature for several values of volume fraction of SiC. The solid curve at the top of the plot is for pure aluminum: the data are from Volume 12 of Reference [23]. The light and dark gray bars summarize measurements made by Mr. Sanford (Code 313, GSFC)for 20% SiC and 40% SiC, respectively. The open circle and closed circle with error bars, at 22 °C, were supplied by GE for 20% SiC and 40% SiC, respectively. The remaining open circles and closed circles are from Reference [14] for 20% SiC and 40% SiC, respectively.

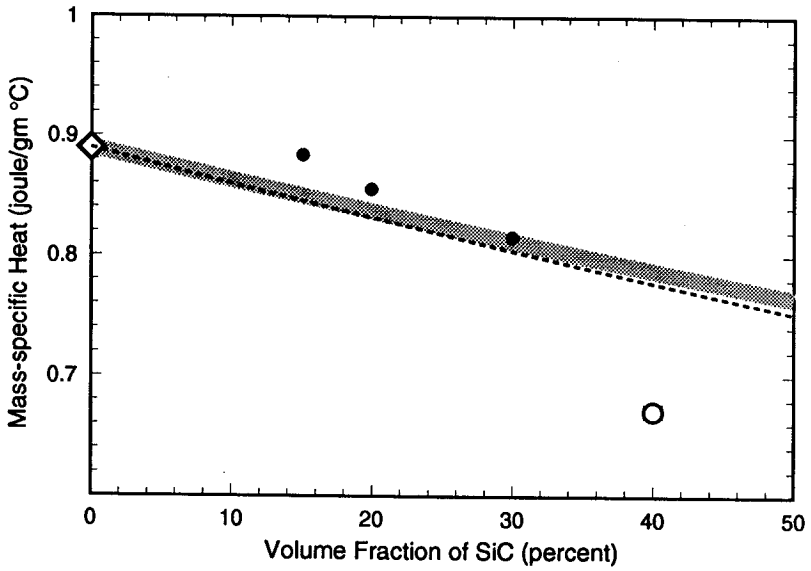

Figure 4.2: The mass specific heat of Al+SiC at 25 °C versus SiC fraction. The value for pure aluminum is shown as a diamond at zero SiC content: the data are from Volume 12 of Reference [23]. The closed circles are from Reference [14]. The open circle for 40% SiC was supplied by GE. The continuous curves are computed using the simple mixing model and the value 0.661 joule/(g °C) for pure SiC at 22 °C; this also is from Reference [23]. The gray band is for $\mathcal{VF}_{\text{void}} = 0\%$ and the dotted line is for $\mathcal{VF}_{\text{void}} = 10\%$.

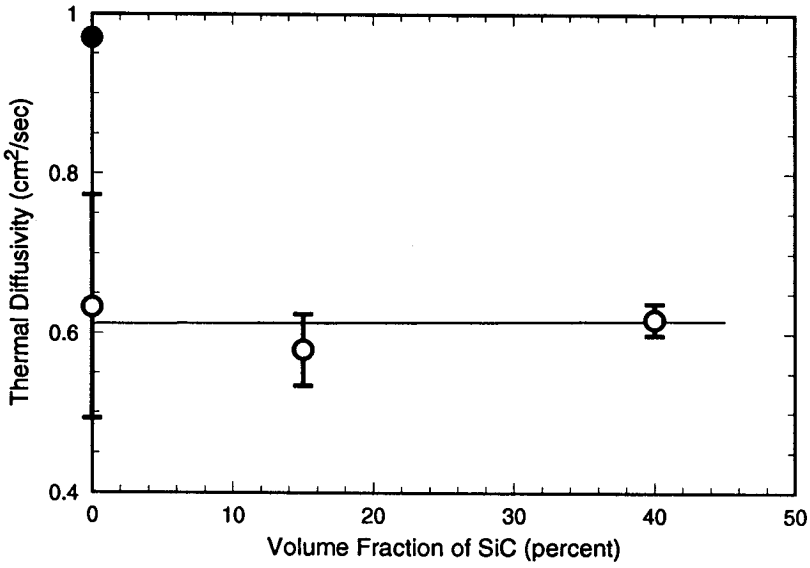

Figure 4.3: The thermal diffusivity of Al+SiC at 25 °C versus SiC fraction, for 6061 aluminum. The data are from References [3, 4, 14], and GE. Also shown as a filled disk is the value for pure aluminum reported by Volume 10 of Reference [23].

roughly 5%. Thus,

$$c^{[m]} = x_{\mathrm{Al}}^{[m]} \cdot c_{\mathrm{Al}}^{[m]} + x_{\mathrm{SiC}}^{[m]} c_{\mathrm{SiC}}^{[m]} \,, \tag{4.1}$$

where $x_{\mathrm{Al}}^{[m]}$ is the mass fraction of aluminum (etc.), and

$$1 = x_{\mathrm{Al}}^{[m]} + x_{\mathrm{SiC}}^{[m]} + x_{\mathrm{void}}^{[m]} \,. \tag{4.2}$$

Expressing this in terms of the volume fraction of the silicon carbide fraction and of the voids, we have

$$c^{[m]} = \frac{c_{\mathrm{Al}}^{[m]}}{1 + \frac{\rho_{\mathrm{SiC}} \mathcal{VF}_{\mathrm{SiC}}}{\rho_{\mathrm{Al}} (1 - \mathcal{VF}_{\mathrm{SiC}} - \mathcal{VF}_{\mathrm{void}})}} + \frac{c_{\mathrm{SiC}}^{[m]}}{1 + \frac{\rho_{\mathrm{Al}} (1 - \mathcal{VF}_{\mathrm{SiC}} - \mathcal{VF}_{\mathrm{void}})}{\rho_{\mathrm{SiC}} \mathcal{VF}_{\mathrm{SiC}}}} \,. \tag{4.3}$$

Indeed, the data reported in Reference [14] agree with the mixing rule to within 4% or better. However, the value reported by GE is some 15% lower than the estimate provided by the mixing rule estimate. Since the actual volume fraction of the voids is $(1.4 \pm 0.2)\%$ for this material, then this discrepancy is not caused by void content.

There is no reliable model for computing the thermal diffusivity of the composite from its constituents, nor are reliable values available for the individual constituents; thus, we must rely on data alone. Certain general principles apply and allow some sense to be made of the observed trends. The thermal diffusivity κ_{td} of a metal is a sensitive function of the mobility of its conduction electrons; this mobility decreases as the lattice is made irregular by the introduction of alloying metals or defects. The thermal diffusivity of single crystal pure aluminum is 0.92 cm^2/s at 25 °C. This drops to 0.82 cm^2/s for sheet annealed 6061 alloy and to 0.74 cm^2/s for heat-treated 6061 alloy. (The purpose of the heat treatment is to produce controlled precipitation of the low concentration-alloyed materials to arrest the motion of dislocations.) Cold working the heat-treated

alloy introduces dislocations which reduce the mobility of the electrons. Thus the appropriate reference value for 6061 aluminum with zero volume fraction of silicon carbide is about 0.62 cm^2/s as shown in Figure 4.3, since the aluminum in the composite is cold-worked during consolidation.

The thermal conductivity of silicon carbide single crystals is in the range 0.5 to 5 watts/(cm °C) at 22 °C depending on crystalline perfection (see Volume 2 of [23]), and so the thermal diffusivity is in the range 0.2 to 2 cm^2/sec. Thus, addition of silicon carbide to aluminum can either lower the thermal diffusivity or raise it, depending on the particular choice of the starting materials; the range of variation is roughly a half order of magnitude. The results shown in Figure 4.3 indicate almost no change at all in thermal conductivity as silicon carbide is added: this result is presumably sensitive to the choice of the particular silicon carbide and aluminum that is used.

These data allow computation of the Zener damping. See Table 4.1 for the values of g_{Max} and f_{Zener}, along with the values chosen for the properties discussed in the previous paragraph. (In this Table, the volume specific heat is computed from the mass specific heat and the density: $c = c^{[m]}\rho$, values for the density ρ and the thickness h are in Table 3.1, and values for Young's modulus are in Table 5.1.) The variation of g_{Max} with $\mathcal{VF}_{\text{SiC}}$ is found to be weak. This is because the increase in E is compensated by the decease in α^2. Hence, the Zener damping of these composites is about the same as for the base aluminum itself.

Table 4.1: Thermal Expansion α, Volume Specific Heat c, Thermal Diffusivity κ_{th}, and the Zener Damping Constants g_{Max} and f_{Zener}

Beam	α ($\frac{10^{-6}}{°C}$)	c ($10^7 \frac{\text{erg}}{\text{cc}\,°C}$)	κ_{th} (cm^2/sec)	g_{Max} (dimensionless)	f_{Zener} (Hz)	
CONTROL	23.2 ± 0.5	2.41 ± 0.04	0.65 ± 0.10	$0.002\,27 \pm 3\%$	40	$\pm 15\%$
GRAY	14.9 ± 0.9	2.33 ± 0.09	0.59 ± 0.05	$0.001\,60 \pm 7\%$	23	$\pm 10\%$
THICK	12.5 ± 0.8	2.24 ± 0.13	0.62 ± 0.03	$0.001\,53 \pm 9\%$	2.0	$\pm$ 5%
MEDIUM	12.5 ± 0.8	2.24 ± 0.13	0.62 ± 0.03	$0.001\,53 \pm 9\%$	20	$\pm$ 5%
THIN	12.5 ± 0.8	2.24 ± 0.13	0.62 ± 0.03	$0.001\,53 \pm 9\%$	183	$\pm$ 5%

Chapter 5

Results and comparisons with literature

Elastic moduli were calculated as discussed in Appendix A and are shown in Table 5.1 and in Figure 5.1. The Timoshenko corrections to the transverse vibration spectra were appreciable for all but the THIN beam. The moduli determined from each of the frequency spectra for each of the 40% SiC_P beams are consistent, and so only the weighted averages and uncertainties are listed in Table 5.1. For the 20% SiC_W beam, the shear modulus G and Poisson's ratio were not determined because the GRAY beam was slightly bent, which prevented interpretation of the torsional modes using the formulae of Appendix A.

The results for Young's modulus agree with those obtained using conventional stress-strain methods [9] shown in Figure 5.1.

The transverse damping of the THIN beam (#4; 40% SiC_P) shown in Figure 5.2 is dominated by Zener damping. This is shown by the agreement between the measured data and the theoretical Zener damping curve computed from Equation C.3 with *no* adjustable parameters. The curve shown in Figure 5.2 was not adjusted to fit the data displayed there, but was computed from the measured thermoelastic properties and beam dimensions. The differences between the experimental and theoretical curves visible at the lower frequencies shown in Figure 5.2 have been traced to an

Table 5.1: Elastic Moduli Computed from Vibrational Frequencies, and Poisson's Ratio Computed from $E/(2G) - 1$

Composition	E (10^{11} dynes/cm^2)	G (10^{11} dynes/cm^2)	Poisson's ratio $= E/(2G) - 1$
Al	6.9 ± 0.1	$\star$	$\star$
Al+20% SiC_W	11.4 ± 0.1	$\star$	$\star$
Al+40% SiC_P	14.9 ± 0.1	5.60 ± 0.03	0.31 ± 0.01

Note: Cases for which there are no measurements are marked with a star ($\star$).

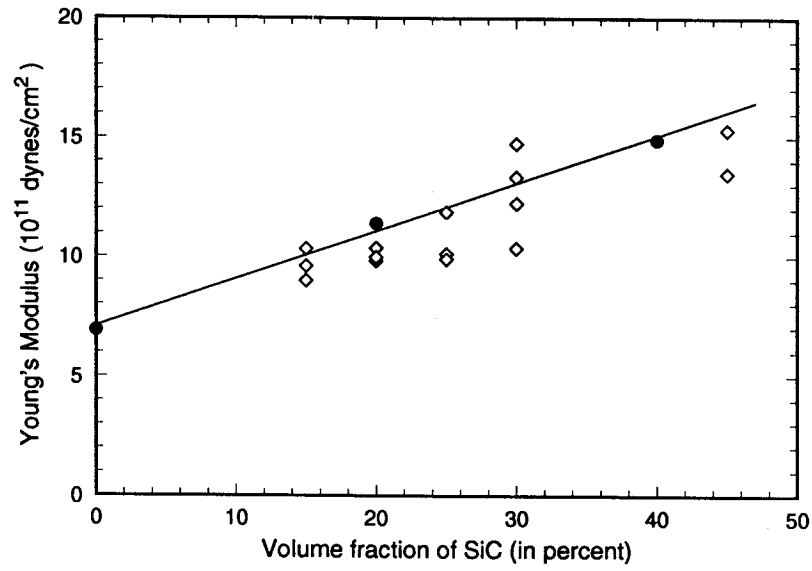

Figure 5.1: Young's modulus versus SiC concentration. Data from this report are shown as filled circles and from Reference [14] are shown as open circles. The straight line is a linear fit to the filled circles only.

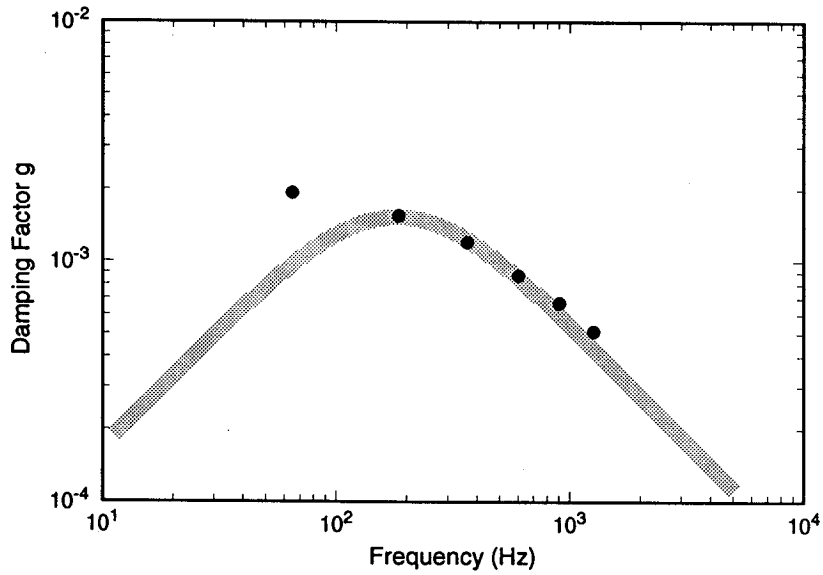

Figure 5.2: The observed transverse damping versus frequency for the THIN beam, together with the Zener damping. The width of the gray curve for the Zener damping reflects its uncertainty caused by the uncertainties in the thermal and mechanical quantities used to compute it.

unstiffening effect provided by the electromagnetic driver and sensor: these devices were found to intrude on the motion of this beam by providing a negative spring constant. This showed up in the details of the frequency spectrum as well: the lowest frequency was displaced upwards by several Hertz.

Results for all transverse modes are shown in Figure 5.3. The data are normalized by scaling the observed damping by the Zener damping and the actual frequency by the Zener frequency. Zener damping is seen to describe the observed damping until the scaled frequency differs by more than an order of magnitude from the Zener frequency. Then a second sort of damping, roughly independent of frequency, becomes visible. This excess damping, $g_{\text{obs}} - g_{\text{Zener}}$, is more clearly visible when it is plotted directly: this is done in Figure 5.4.

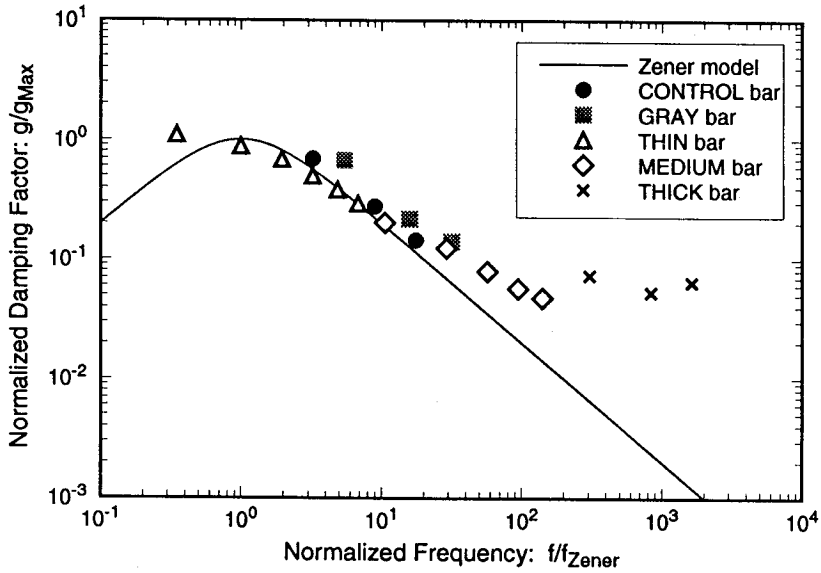

Figure 5.3: The scaled transverse damping versus frequency for all beams. The observed damping is divided by the Zener damping and the observed frequency is divided by the Zener frequency.

The Zener damping of aluminum is substantially unchanged by the addition of silicon carbide: the decrease in the thermal expansion α compensates the increase in the Young's modulus E. We do not know what is causing the other (i. e., the excess) damping. It is not present in aluminum beams that do not contain SiC, so it is certainly caused by the SiC. Since the specimen with 20% SiC_{W} shows about as much damping as the specimens with 40% SiC_{P}, whiskers may be more effective than particulate SiC in producing damping. Perhaps this excess damping is simply another instance of Zener damping caused by thermal currents, where the heating is at the Al/SiC interface during beam deformation (it is the aluminum that deforms—the silicon carbide does not), and the relevant currents flow through and around the SiC phase, as well as between neighboring SiC inclusions; hence, a broad distribution of thermal relaxation times would be expected.

Ms. Timmerman et al. [20, 14] have measured the transverse vibrational frequencies and damping of Al+SiC beams using a method similar with the one described here. The Young's moduli are in agreement with this work. They consistently measure a greater damping factor than reported here; however, their experiments were carried out in air. They did not analyze their results in terms of Zener's damping mechanism. They did not consider longitudinal and transverse vibrations and associated dampings.

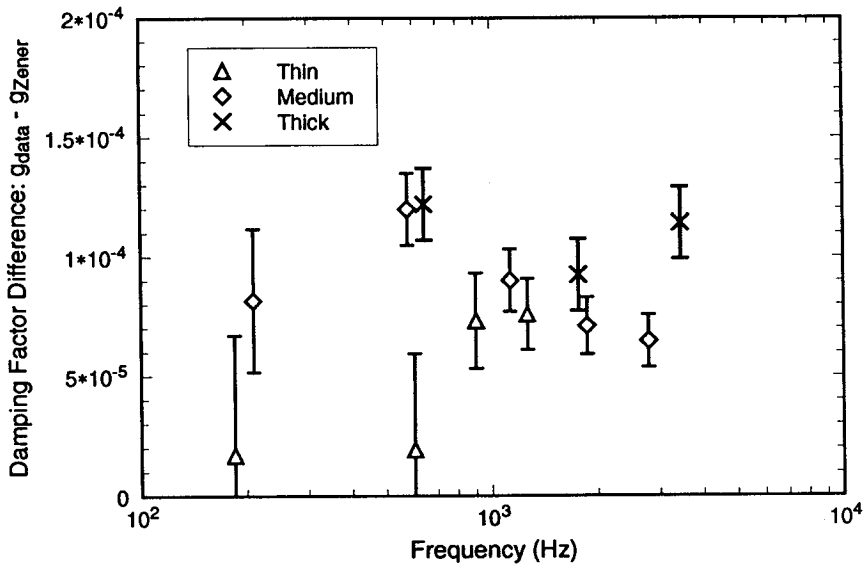

Figure 5.4: The computed excess transverse damping versus frequency for the 40% SiC beams.

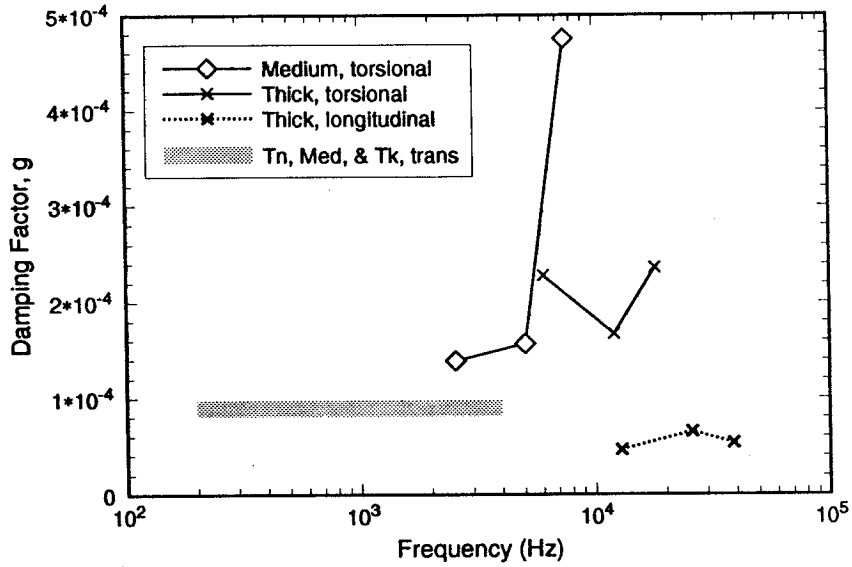

Figure 5.5: The observed damping versus frequency for the torsional modes of the MEDIUM and THICK beams, and the longitudinal modes of the THICK beam. The excess damping of the transverse modes of the THIN, MEDIUM, and THICK beams is summarized as a gray band whose width measures the scatter in these values.

Chapter 6

Conclusions

Material damping can be important for orbital operations requiring control of vibrations. The material damping of the transverse vibrations of aluminum beams shows a Zener damping part which varies with the beam thickness and vibration frequency and can be as large as $g \approx 2 \times 10^{-3}$ at one particular frequency, the *Zener frequency*, which depends upon the beam's thickness. Zener damping g_{Zener} drops as the beam's transverse frequency departs from the Zener frequency in either direction, and eventually some other kind of damping will become visible.

For aluminum reinforced with discontinuous silicon carbide in the form of whiskers or powders, the Zener contribution to the transverse vibrational damping is almost unchanged from that of the base aluminum alloy. However, there is an excess damping which is roughly independent of frequency and modal type, with $g \approx 10^{-4}$. Hence it can be misleading to use a single handbook value of g without regard to the frequency or to the modal type (i.e., longitudinal, torsional, or transverse deformations).

Bibliography

Timoshenko, Stephen P., 1921, "LXVI. On the correction for shear of the differential equation for transverse vibrations of prismatic bars," *Philosophical Magazine*, Series 6, 41, pp. 744–746. Reprinted in **Vibration: Beams, Plates, and Shells**, edited by Arturs Kalnins and Clive L. Dym, published in 1976 by Dowden, Hutchinson & Ross, Inc., Stroudsburg, PA.

Pickett, Gerald, 1945, "Equations for computing elastic constants from flexural and torsional resonant frequencies of vibration of prisms and cylinders," Proceedings, *Am. Soc. Testing Materials*, 45, pp. 846–865.

Strutt, John William, 3^{d} Baron Rayleigh, 1945, *The Theory Of Sound*, Dover Publications, New York, First American edition. First edition: London, Vol. 1 in 1877 and Vol. 2 in 1878; second edition: London, Vol. 1 in 1894 and Vol. 2 in 1896.

Zener, Clarence, 1948, *Elasticity and Anelasticity of Metals*, The University of Chicago Press, Chicago, Illinois.

Timoshenko, Stephen P., D. H. Young, and W. Weaver, Jr., 1955, *Vibration Problems in Engineering*, John Wiley & Sons, New York, third edition.

Mindlin, R. D., and H. Deresiewicz, 1955, "Timoshenko's shear coefficient for flexural vibrations of beams," *Proceedings of the Second U. S. National Congress of Applied Mechanics*, pp. 175–178, The American Society of Mechanical Engineers. Reprinted in **Vibration: Beams, Plates, and Shells**, edited by Arturs Kalnins and Clive L. Dym, published in 1976 by Dowden, Hutchinson & Ross, Inc., Stroudsburg, PA.

Spinner, Sam, and Rudolph C. Valore, Jr., 1958, "Comparison of theoretical and empirical relations between the shear modulus and torsional resonance frequencies for bars of rectangular cross section," *Journal of Research of the National Bureau of Standards*, 60(5), pp. 459–464.

Spinner, S., T. W. Reichard, and W. E. Tefft, 1960, "A comparison of experimental and theoretical relations between Young's modulus and the flexural and longitudinal resonance frequencies of uniform bars," *Journal of Research of the National Bureau of Standards*, 64A(2), pp. 147–155.

Spinner, Sam, and Wayne E. Tefft, 1961, "A method for determining mechanical resonance frequencies and for calculating elastic moduli from these frequencies," *Proceedings, American Society for Testing and Materials*, 61, pp. 1221–1238.

Harris, Cyril M., and Charles E. Crede, editors, 1961, *Shock and Vibration Handbook*, Volume 2, pp. (37)1–(37)34, McGraw-Hill Book Company, New York.

Tefft, Wayne E., and Sam Spinner, 1962, "Cross-sectional correction for computing Young's mod-

ulus from longitudinal resonance vibrations of square and cylindrical rods," *Journal of Research of the National Bureau of Standards*, 66A(2), pp. 193–197.

Granick, Neal, and Jesse E. Stern, 1965, *Material Damping of Aluminum by a Resonant-Dwell Technique*, NASA TN D-2893.

(anonymous), 1971, *Investigation of Techniques for Determining Damping Characteristics of Large Flexible Spacecraft Undergoing Small Amplitude Oscillations*, Final Report on "Contract NAS5-11822 PC 733-W37513," 746-FR-621-001, Fairchild Industries, Incorporated, Germantown, MD, October 1971. Prepared for NASA/GSFC.

Touloukian, Y. S., R. K. Kirby, R. E. Taylor, and P. D. Desai, 1973, *Thermophysical Properties of Matter*, IFI/Plenum, New York and Washington.

Crawley, F., George L. Server, and David G. Mohr, 1983, "Experimental measurements of passive material and structural damping for flexible space structures," *Acta Astronautica*, 10(5-6), pp. 381–393. Reprinted in *Vibration Damping 1984 Workshop Proceedings*, pp. A23–A35, Lynn Rogers, ed., Flight Dynamics Laboratory, Air Force Wright Aeronautical Laboratories, Wright-Paterson Air Force Base, Ohio 45433.

Mar, James W, 1984, "Some musings on how to make damping a creative force in design," *Vibration Damping 1984 Workshop Proceedings*, Lynn Rogers, ed., pp. A2–A7, Flight Dynamics Laboratory, Air Force Wright Aeronautical Laboratories, Wright-Paterson Air Force Base, Ohio 45433.

Jensen, D. L., 1984, "Structural damping of shuttle orbiter and ascent vehicles," *Vibration Damping 1984 Workshop Proceedings*, Lynn Rogers, ed., pp. Z2–Z14, Flight Dynamics Laboratory, Air Force Wright Aeronautical Laboratories, Wright-Paterson Air Force Base, Ohio 45433.

Schoutens, J., 1984, "Simple and precise measurements of fibre volume and void fractions in metal matrix composite materials," *Journal Of Materials Science*, 19, pp. 957–964.

Sudey, J. Jr., and J. R. Schulman, 1984, "In orbit measurements of Landsat-4 Thematic Mapper dynamic disturbances," 35th *Congress of the International Astronautical Federation*, American Institute of Aeronautics and Astronautics, 1633 Broadway, New York, NY 10019; IAF-84-117.

Timmerman, Nancy S., and John Doherty, 1984, *Loss Factors Measured in Metal Matrix Composite Materials*, Final Report on "Contract No. DAAG46-82-C-0060," AMMRC TR 84-22, Bolt Beranek and Newman Inc., 10 Moulton Street, Cambridge, MA 02138, June 1984. Prepared for the Army Materials and Mechanics Research Center. Approved for public release; distribution unlimited.

Schoutens, Jacques E., 1984, "Discontinuous Silicon Carbide Reinforced Aluminum Metal Matrix Composites Data Review," in *MMCIAC Databook Series* MMCIAC No. 000461, DOD Metal Matrix Composites Information Analysis Center, 816 State Street, PO Drawer QQ, Santa Barbara, CA 93102.

McDanels, D., 1985, "Analysis of stress-strain, fracture, and ductility behavior of aluminum matrix composites containing discontinuous silicon carbide reinforcement," *Metallurgical Transactions A*, 16A, pp. 1105–1115.

C 215-85, 1986, "Standard test method for fundamental transverse, longitudinal, and torsional frequencies of concrete specimens," in *Annual Book of ASTM Standards*, ASTM, 1916 Race Street,

Philadelphia, PA.

Rao, M. Sambasiva, and P. S. Nair, and S. Durvasula, 1986, "Equivalent dynamic models for a spacecraft and its subsystems," *ESA Journal*, 10(1), pp. 93–111.

Wren, Graeme G., and Vikram K. Kinra, 1988, "An experimental technique for determining a measure of structural damping," *Journal of Testing and Evaluation*, 16(1), pp. 77–85.

Appendix A

The vibration of thin beams

The vibration spectrum of a beam has been studied for centuries, and we now know that there are no exact formulae that we can use to reduce the experimental data obtained above; rather, we must use approximations. The purpose of this section is to present some useful approximations.

When the material is idealized as perfectly elastic and linear, and air loading and support loading are ignored, then the theory of elasticity provides the equations of motion. Then the ignored loadings can be reintroduced by means of perturbation theory. No exact solutions to even the simplified, idealized equations have been found. The current approach is to use the solution to the *thin uniform beam* equations that predate the theory of elasticity, and to multiply this solution by a series of correction terms. The nature of the correction terms is guided by approximate results from the theory of elasticity, but the actual values are taken from experiment. The situation is even less fundamentally founded when more realistic material models are used, such as those involving anelasticity (e.g., damping) and nonlinearity.

A.1 Transverse vibrations

Thin beam theory supposes that the shape of the beam is accurately described when the vertical displacement of its midline η is known for each position x from one end to the other; i. e., when $\eta(x)$ is known over the interval $-\ell/2 \leq x \leq +\ell/2$. And it supposes that this displacement is described by the equation of motion

$$\rho A \left(\frac{\partial^2 \eta}{\partial t^2} \right) = - \left(\frac{\partial^2}{\partial x^2} \, EI \left(\frac{\partial^2 \eta}{\partial x^2} \right) \right) \, , \tag{A.1}$$

where all support forces and air damping forces are ignored, and where E is Young's modulus, I is the geometrical moment of inertia, ρ is the mass density, and A is the cross section area.

A.1.1 Uniform thin beam theory

The *Uniform Thin Beam* (UTB) model corresponds to the important case that the beam's properties are uniform over its length, or at least that EI and ρA are uniform. Then the solutions

are linear combinations of the spatial trig and hyperbolic trig functions, $\cos(kx), \sin(kx), \cosh(kx)$, and $\sinh(kx)$, multiplied by a linear combination of the temporal trig functions, $\cos(2\pi ft)$ and $\sin(2\pi ft)$, where k is the wave number and f is the frequency.

We are interested in the case in which both ends of the beam are free. Thus, there is no bending moment at either end ($\partial^2\eta/\partial x^2$ vanishes at each end), and there is no shearing force at either end ($\partial^3\eta/\partial x^3$ vanishes at each end). It is then convenient to work with the normalized wave number $\kappa = k\ell$, since it is dimensionless.

The symmetric solutions are

$$\eta_p^{[s]}(x,t) = \mathcal{A} \cdot \left[\frac{\cos(\kappa_p^{[s]} x/\ell)}{\cos(\kappa_p^{[s]}/2)} + \frac{\cosh(\kappa_p^{[s]} x/\ell)}{\cosh(\kappa_p^{[s]}/2)} \right] \cdot \sin(2\pi f_p^{[s]} t + \phi) \ , \tag{A.2}$$

where $\kappa_p^{[s]}$ is the normalized wave number of the p^{th} symmetric mode and $f_p^{[s]}$ is the frequency of this mode. The amplitude $\mathcal{A}$ and phase factor ϕ are determined by initial conditions. The normalized wave number for the symmetric modes satisfies the equation

$$\tan(\kappa_p^{[s]}/2) + \tanh(\kappa_p^{[s]}/2) = 0 \, ; \tag{A.3}$$

the roots of this equation cannot be found exactly using analytic methods; rather, numerical methods must be used. Values for the first two p modes are shown in Table A.1. This table also contains the antisymmetric results. Both results are reported both in symmetric, or antisymmetric, form using the p mode number and also without regard to symmetry by using the n mode number. The approximate expression

$$(\kappa_p^{[s]})_{app} = (4p-1) \cdot (\pi/2) \tag{A.4}$$

is accurate to better than six significant figures for $p > 2$, and so tabled values are not needed then. The last column of Table A.1 shows the rate at which κ_n converges to this approximate expression, and shows that the symmetric and antisymmetric values approach this approximate expression's values from opposite sides.

The nodal lines are then found as the roots of the symmetric solutions given by Equation A.2. It is experimentally convenient to describe the position of each nodal line by its distance inward from the end of the beam; thus, the q^{th} node of the p^{th} mode is at $\phi_{p,q}^{[s]} \cdot \ell$, measured inward from the end of the beam, where $\phi_{p,q}^{[s]}$ is dimensionless. The dimensionless fraction is zero at the end of the beam, $\phi = 0$, and is one half at the middle of the beam, , $\phi = 1/2$. The dimensionless locations are shown in Table A.2 for the first two symmetric modes. This table also contains the antisymmetric results, and expresses these both using the p mode number and also without regard to symmetry by using the n mode number. An approximate expression for $\phi_{p,q}^{[s]}$ is

$$(\phi_{p,q}^{[s]})_{app} = (2q - 3/2)/(4p-1) \quad \text{where } q = 1, 2, \ldots, p \ , \tag{A.5}$$

where $q = 1$ corresponds to the outermost nodal line, and $q = p$ corresponds to the innermost one. This is sufficiently accurate that it can be used to extend the Table when this is necessary.

The antisymmetric solutions are

$$\eta_p^{[a]}(x,t) = \mathcal{A} \cdot \left[\frac{\sin(\kappa_p^{[a]} x/\ell)}{\sin(\kappa_p^{[a]}/2)} + \frac{\sinh(\kappa_p^{[a]} x/\ell)}{\sinh(\kappa_p^{[a]}/2)} \right] \cdot \sin(2\pi f_p^{[a]} t + \phi) \ , \tag{A.6}$$

Table A.1: Normalized Wave Numbers for the First Four Modes

n-mode	p-mode	$\kappa_p^{[s]}$	$\kappa_p^{[a]}$	$\kappa_n \cdot (2/\pi)$
1	1, s	4.730 041		3.011 237
2	1, a		7.856 205	4.999 505
3	2, s	10.995 608		7.000 021
4	2, a		14.137 165	8.999 999

Table A.2: Normalized Positions of the Nodes of the First Four Modes

n-mode	p-mode	$\phi_{p,q}^{[s]}$	$\phi_{p,q}^{[a]}$
1	1,s	0.2242	
2	1,a		0.1321, 0.5000
3	2,s	0.0944, 0.3558	
4	2,a		0.0736, 0.2768, 0.5000

where $\kappa_p^{[a]}$ is the normalized wave number of the p^{th} antisymmetric mode and $f_p^{[a]}$ is the frequency of this mode. The amplitude $\mathcal{A}$ and phase factor ϕ are determined by initial conditions. The normalized wave number for the antisymmetric modes satisfies the equation

$$\tan(\kappa_p^{[a]}/2) - \tanh(\kappa_p^{[a]}/2) = 0\,; \tag{A.7}$$

the roots of this equation cannot be found exactly using analytic methods; rather, numerical methods must be used. Values for the first two p modes are shown in Table A.1. These are reported both in symmetric/antisymmetric form using the p mode number and also without regard to symmetry using the n mode number. The approximate expression

$$(\kappa_p^{[a]})_{app} = (4p+1)\cdot(\pi/2) \tag{A.8}$$

is accurate to better than six significant figures for $p > 2$.

The nodal lines are then found as the roots of the antisymmetric solution. These are shown in Table A.2 for the first two antisymmetric modes. An approximate expression for these roots is

$$(\phi_{p,q}^{[a]})_{app} = (2q-3/2)/(4p+1) \quad \text{where } q = 1, 2, \ldots, p+1\ , \tag{A.9}$$

where $q = 1$ corresponds to the outermost nodal line and $q = p+1$, the innermost one (which is always precisely at the middle of the beam: $\phi_{p,p+1}^{[a]} = 1/2$).

For the outermost node, $q = 1$, the correct position is always larger than the approximate one; for $p > 2$, the value $1.322 \times (\phi_{p,1})_{app}$ is accurate to the given number of figures for both the symmetric and antisymmetric cases. For the next node, $q = 2$, the value $0.9962 \times (\phi_{p,2})_{app}$ for $p > 2$ is accurate to the given number of figures for both the symmetric and antisymmetric cases. The errors for $q > 2$ are less than 0.009% for both symmetric and antisymmetric cases.

These nodal lines, at each of which the amplitude of vibration vanishes, can be reliably located by gently touching the beam at trial locations while it is in oscillation; only when the beam is touched

at a nodal line will it continue to oscillate. The mode number n can be determined in this way for any given mode of oscillation.

The vibrational spectrum of a uniform thin beam (UTB) suspended at its nodal lines is

$$f_n^{\text{UTB}} = \left(\frac{1}{2\pi}\frac{r_g}{\ell^2}\sqrt{\frac{E}{\rho}}\right)\cdot\kappa_n^2\ , \tag{A.10}$$

where r_g = radius of gyration = $\sqrt{I/A}$ in general, and $r_g = h/\sqrt{12}$ for a beam with rectangular cross section and a thickness h. (The other quantities have been defined earlier in this section.)

A.1.2 Rayleigh's perturbation theory for thin beams

Rayleigh's perturbation theory[1] is useful when the beam is not perfectly uniform:

$$f_n = f_n^{UTB}\cdot\sqrt{1+\frac{\int\delta(EI)\cdot(u_n'')^2\,dx}{(EI)\int(u_n'')^2\,dx}-\frac{\int\delta(\rho A)\cdot u_n^2\,dx}{(\rho A)\int u_n^2\,dx}}\ , \tag{A.11}$$

where

E is Young's modulus,

I is the beam's geometrical moment of inertia,

ρ is the beam's mass density,

A is the cross sectional area of the beam,

$q_0 = \int_{-\ell/2}^{+\ell/2} q(x)\,dx/\ell$ is the beam-averaged value of $q(x)$, and $\delta q = q(x) - q_0$ is the deviation from this average, where q is either EI or ρA,

$u_n(x)$ = transverse displacement of beam at the position x in the n^{th} mode when calculated for a uniform thin beam with $(EI)_0$ and $(\rho A)_0$, and

$u'' = \partial^2 u/\partial x^2$.

In particular, it follows from Equation A.11 that attaching the masses m_ℓ and m_{r} at the left and right tips of a beam of mass m_{beam} will lower all frequencies. In practice, these masses are not mounted precisely at the tips, but a distance δ inwards from the tips. The new frequency is

$$f_{n,\delta m} = f_n^{\text{UTB}}\cdot\sqrt{1-[4-\alpha_n\,\chi_n+\beta_n\,\chi_n^2+\cdots]\cdot\left[\frac{m_\ell+m_{\text{r}}}{m_{\text{beam}}}\right]}\ ,$$

where $\chi_n = \delta/(\phi_{n,1}\,\ell)$ is the ratio of the inward distance of the masses m_ℓ, m_{r} to the first nodal line in the n^{th} mode. This result is only valid as long as the masses are closer to the tip than the first nodal line. The dimensionless coefficients depend on n, but weakly enough so that we can use $\alpha_n = 8.31$ and $\beta_n = 4.31$ for all n, for all practical purposes. The tips of the beam execute a greater motion than any other part of the beam since they are free, and so adding mass there is

[1] See Equation 1 in §185 on page 292 of Volume 1, [7].

especially effective in lowering the frequency of the beam. This is the reason for the factor "4." As the mode number increases, the nodal line approaches the location of the masses m_ℓ, m_r at $\delta > 0$, so the effect of these masses decreases. This is the reason for the $-\alpha_n \chi_n$ term. Indeed, the masses m_ℓ, m_r have no effect at all in the context of this model[2] when they are located at the nodal line. The $\beta_n \chi_n^2$ term corrects the linear effect described by $\alpha_n \chi_n$ to give a better description of the location of the nodal line.

Some thin beams are not uniform in their properties. Then the frequency spectrum is not described by Equation A.10, but Equation A.11 can be used to carry out a kind of fourier analysis[3] of the distribution of the irregularities along the beam. This was not necessary for the beams considered in this report and so will not be developed further here.

A.1.3 Timoshenko beam theory

Sometimes a beam is not thin enough for the UTB model to provide an accurate description of its vibration spectrum. As the thickness increases, the effects of rotational motions and shear deformations become important. The extension of classical thin beam theory to include these effects is called *Timoshenko beam theory* (TIM).[4]

Timoshenko showed that the frequency of the n^{th} mode of a beam whose ends are both pinned is

$$(f_n)^{\text{TIM,PP}} = (f_n)^{\text{UTB,PP}} \cdot \sqrt{1 - \left(1 + \frac{E}{\mathcal{K}_{\text{TIM}}\, G}\right) \left(\frac{\kappa_n^{[\text{PP}]} r_g}{\ell}\right)^2 + \mathcal{O}(k_{+,n}^4)}\ , \qquad \text{(A.12)}$$

where $(f_n)^{\text{UTB,PP}} = [(EI)/(\rho A)]^{1/2}\ (\kappa_n^{[\text{PP}]}/\ell)^2$ is the frequency of the n^{th} mode of a pinned-pinned uniform thin beam, and $\kappa_n^{[\text{PP}]} = k_{+,n}\ell = \pi, 2\pi, \ldots, n\pi$ where $n = 1, 2, \ldots$ is the n mode number. The [PP] superscript denotes "pinned-pinned" end conditions.

Since the radius of gyration r_g is proportional to the thickness of the beam, and since $\ell/\kappa_n = 1/k_n = 2\pi\lambda_n$ is the wavelength of the n^{th} mode, then $(\kappa_n r_g/\ell)^2 = [r_g/(2\pi\lambda_n)]^2$; thus, the thin beam results are recovered as the ratio of thickness to wavelength vanishes. And, for nonvanishing thickness, the frequencies are lowered below the thin beam values as the wavelength decreases, i. e., as the frequency increases.

Analysis of our data requires the frequencies of a beam whose ends are both free. The result has the same form as Equation A.12, but the numerical values of the κ_n are different. Timoshenko's model explains the way in which the observed frequencies of real beams are lower than those given by the Uniform Thin Beam model. In practice, it is most convenient to fit the observed data to an expression of the form of Equation A.12, and to extrapolate this to vanishing frequency; this gives $(f_n)^{\text{UTB}}$, which is then used to determine E/ρ.

[2]The masses are fastened to the outside of the beam and so they augment its rotational kinetic energy even when located at nodal locations since the slope is oscillating at nodal lines. The rotational kinetic energy is of order $(h/\ell)^2$ and so is ignored for thin beams. Timoshenko's treatment (see the following) includes the rotational kinetic energy of the beam and thus gives a context for treating this effect which could be visible under certain circumstances.

[3]The analysis uses the orthogonal family $\{\eta_p^{[s]}(x), \eta_p^{[a]}(x)\,; p = 1, 2, \ldots\}$ rather than the trig functions used by Fourier.

[4]Timoshenko independently developed his treatment, publishing it in English in 1921 (see [21]) and again in his influential texts, including [22]. He later found that it had been independently developed several times, as early as 1859 (see [10]), and then gave full credit to his predecessors. The treatment is still called Timoshenko beam theory.

Both Timoshenko effects and nonuniform effects were observed for the specimens we tested, but these effects were small enough to be independent. This permitted each correction to be applied in turn to relate the observed frequency spectrum to the Young's modulus.

A.2 Longitudinal vibrations

Elementary theory predicts a simple result for the longitudinal spectrum of a uniform beam when it is suspended at its nodal lines:

$$f_n^{\mathrm{UTB}} = \frac{n}{2\ell}\sqrt{\frac{E}{\rho}}\,, \tag{A.13}$$

where

$n = n^{\mathrm{th}}$ mode number,

ℓ = length of the beam,

E = Young's modulus, and

ρ = mass density.

As for the case of transverse vibrations, longitudinal vibrations also require corrections because of the thickness of practical beams, and because of deviations from uniformity. These are reported in [7] and [11].

A.3 Torsional vibrations

Elementary theory predicts a simple result for the torsional spectrum of a uniform beam of circular cross section when it is suspended at nodal lines:

$$f_n^{\mathrm{UTB}} = \frac{n}{2\ell}\sqrt{\frac{G}{\rho}}\,, \tag{A.14}$$

where

$n = n^{\mathrm{th}}$ mode number,

ℓ = length of the beam,

G = the shear modulus, and

ρ = mass density.

Results for a rectangular cross section are not elementary. These results, as well as corrections caused by deviations from uniformity, are given in [7] and [11].

Appendix B

Measures of damping

Fundamentally, a motion is said to be damped when the mechanical energy associated with that motion is lost to it, going either into some other (macroscopic) motion,[1] or into heat (microscopic motion). The amount of damping is measured in terms of the rate of loss of this energy.

If a complex structure has an equilibrium configuration, then it is often the case that the "many-degree-of-freedom" motions around this configuration can be resolved into the superposition of motions of many "one-degree-of-freedom" systems; each of these is a *simple harmonic oscillator*,[2] and each moves independently of all its siblings. The complex systems that are studied in terms of equivalent simple harmonic oscillators include quantal super strings, nuclei, molecules, buildings, bridges, spacecraft, the Earth (tides and earthquakes), suns, globular clusters, and galaxies. However, this analysis tends to fail when there is damping. For many cases met in practice, frictional forces are proportional to the velocities of the various motions — this is *linear* damping. In almost all cases, linear damping couples the simple harmonic oscillators so that their motions are not independent. Hence, an analysis into simple harmonic oscillators may not be a simplification. (And the situation is even more complicated in many real cases, especially when there are static and sliding friction in joints, since such damping is not a linear function of the velocity.) Even so, the analysis of a complex system into a set of damped simple harmonic oscillators is often still made, at least to provide a vocabulary for speaking of the real motion. And measurements of the damping of the complex system are often related to the motion of damped simple harmonic oscillators.

In the search for quantities that can be most directly related to the behavior of interest, or quantities that can be readily determined, many measures of damping have been used, including

> ψ = specific damping capacity = $\Delta E_{\sim}/\langle E\rangle_{\sim}$ = the ratio of the energy lost during a cycle of sinusoidal oscillation, $\Delta E_{\sim}$, to the average energy stored during that cycle, $\langle E\rangle_{\sim}$.
>
> g (or η) = damping factor (or loss factor), defined in the same way as ψ, except that a factor of 2π is included in the denominator.

[1] The scattering of a sound wave by rigid obstructions is an example: some energy of the sound wave is lost to that wave and transferred into other sound waves, but there is no heating. The motion of a ship through water is another example: some of the ship's energy is transferred into surface water waves; the motion of the ship is damped, but there is no heating through this mechanism.

[2] "Simple" means "one degree of freedom" in this context.

ζ = fraction of critical damping. (But the actual amount of damping required for criticality is rarely obtained experimentally; rather, it is estimated assuming that the simple harmonic oscillator model is valid. Hence, ζ is a computed quantity and not a measured one.)

δ = logarithmic decrement, defined as the natural logarithm of the ratio of a maximum displacement to the previous maximum (or a minimum to the previous minimum) while the system is freely decaying: $\delta = \ln[\mathcal{A}(t_{\max})/\mathcal{A}(t_{\max}+T)]$, where $\mathcal{A}(t)$ is the amplitude of the motion at the time t and T is the period.

M''/M' = ratio of the imaginary part of an appropriate modulus to its real part.

Q_τ = quality factor, defined as $\pi \times$ the number of cycles a freely decaying system oscillates during the time τ that its amplitude decays to $1/e$ of its starting amplitude: $Q_\tau = \pi\tau/T$ where T is the period of oscillation. Other popular but distinct definitions involve the width of the resonance curve obtained during sinusoidally driven motion (Q_W), and the *magnification factor*, which is the ratio of the amplitude at resonance to the amplitude in the limit of low frequency ($Q_\mathcal{M}$).

ϕ = the phase angle by which the response lags the drive, under sinusoidally driven motion. Actually, it is $\tan\phi$ that is usually used.

Studies of the motion of a vibrating *single-degree-of-freedom* system show that its driven motion can be related to its free motion and, hence, that all these measures of damping are related. When the damping force is linear with the velocity of the motion, and when the damping is small, as it is for all the specimens studied here, the interrelations are simple:

$$g = \eta = 2\zeta = \delta/\pi = M''/M' = 1/Q_\tau = 1/Q_W = 1/Q_\mathcal{M} = \tan\phi = \psi/(2\pi). \tag{B.1}$$

When the damping is linear, but becomes larger,[3] the interrelations become complex. Indeed, for critical damping and greater, a freely decaying system no longer oscillates at all, and several of the above measures ($g, \eta, \delta, Q_\tau, Q_W, \psi$) lose their meaning, since they all involve measurements made over a vibration cycle. And $Q_\mathcal{M}$ losses its meaning, since there is no longer any maximum at a resonance. While other definitions can be used under these conditions, there is less agreement among them. Since we will not need them in this study, none will be mentioned here. More importantly, such large damping usually couples vibration modes. Then the relation of the driven motion to the free motion becomes complicated, and is unique for each structure. Hence, the notion of "single mode critical damping" is something of a fantasy for structures with many degrees of freedom with large damping: we will not use ζ. Similar considerations apply for nonlinear damping.

For the beams studied here, the damping is both linear and small. The various modes were independent, as judged by the absence of any spurious frequencies for the driven tests and by the exponential decay over several orders of magnitude for the free-decay tests. The damping factors of each of the various distinct damping mechanisms often (but not always) add when each is small:

$$g_{\text{total}} = g + g' + g'' + \cdots, \tag{B.2}$$

and so g is a more convenient measure than Q:

$$Q_{\text{total}} = \frac{1}{\frac{1}{Q} + \frac{1}{Q'} + \frac{1}{Q''} + \cdots}. \tag{B.3}$$

[3] How large depends entirely upon the precision one requires. For experimental measurements of $\pm$ 10%, the above simple interrelations are usable for $g < 0.3$, the differences decreasing as g^2.

Appendix C

Zener thermoelastic damping

In his classic book *Elasticity And Anelasticity Of Metals* ([25]), Clarence Zener describes a variety of damping mechanisms that operate within metals. One of them, thermoelastic damping, is of special importance to the damping of transverse vibrations. The idea is simple: As the beam flexes, its compressed side heats, and its stretched side cools.[1] Thermal conduction operates to relax the thermal gradient to bring about thermal equilibrium. Relaxation occurs on a time scale

$$\tau \approx \frac{\text{thickness}^2}{\text{thermal diffusivity}}. \tag{C.1}$$

For very fast vibrations, there is no time for thermal flows to redistribute any of the elastically stored energy, and all the elastic energy stored in the bent beam is mechanically available. The adiabatic modulus applies, and there is no absorption. For very slow vibrations, there is enough time for thermal flows to achieve thermal equilibrium (i. e., to completely relax part of the elastically stored energy), and all processes are isothermal. The isothermal modulus applies, and there is no absorption. However, when the time scales of vibration and thermal relaxation are about the same,

$$2\pi f \tau \approx 1, \tag{C.2}$$

then some of the mechanical energy that the beam stores as elastic distortion is converted into heat during the half period that the beam is flexing. Hence, this energy is not available to be converted into mechanical velocity during the next half period. So there is absorption of mechanical energy. Zener showed that the damping factor g is

$$g_{\text{Zener}} = g_{\text{Max}} \cdot \mathcal{D}(\Omega) \tag{C.3}$$

to a good approximation, where

$g_{\text{Max}} = (\alpha^2 ET)/(2c)$,

$\alpha = (1/\ell)\, d\ell/dT = d \ln \ell/dT =$ linear thermal expansion,

$E =$ Young's modulus,

[1] The thermoelastic effect is much greater for gases and so was noticed long ago by Newton who did not understand what he observed; the effect was correctly understood and described by Laplace. Clearly, Zener stood in a noble line when he applied this idea to solids.

T = absolute temperature,

c = volume specific heat capacity,

$\mathcal{D}(\Omega) = 2\Omega/(1+\Omega^2) = 2/(\Omega + 1/\Omega)$ is the Debye relaxation function,

$\Omega = 2\pi f\tau = f/f_{\text{Zener}}$ is a dimensionless frequency,

$\tau = (h/\pi)^2/\kappa_{td}$ is the thermal relaxation time for a rectangular beam of uniform thickness h,

$f_{\text{Zener}} = (\pi/2)(\kappa_{td}/h^2)$ is the frequency of maximum g, and

κ_{td} = thermal diffusivity of the beam.

Zener showed that $g_{\text{Zener}}(f)$ described the damping in a great variety of materials, including many metals (including aluminum) and also glass. Later workers have shown that, at least for frequencies within a decade or so of f_{Zener}, this model describes observed damping to within the accuracy with which the above-listed elastic and thermal properties are known. In some cases, the agreement is to within 5% with no adjustable parameters. Experiments with reeds vibrating in a vacuum show excellent agreement for frequencies as much as a decade below f_{Zener}, as well as above it. Hence, experiments that show g rising above g_{Zener} as the frequency is dropped below f_{Zener} [3] are probably experiencing extraneous damping.

Notes

[1] C 215-85. Standard test method for fundamental transverse, longitudinal, and torsional frequencies of concrete specimens. In *Annual Book of ASTM Standards*, ASTM, 1916 Race Street, Philadelphia, PA, 1986. ... "for the purpose of calculating dynamic moduli of elasticity and of shear, as well as the dynamic Poisson's ratio". Much of this ASTM is actually general, and not restricted to concrete.

[2] (anonymous). *Investigation of Techniques for Determining Damping Characteristics of Large Flexible Spacecraft Undergoing Small Amplitude Oscillations.* Final Report on "Contract NAS5-11822 PC 733-W37513" 746-FR-621-001, Fairchild Industries, Incorporated, Germantown, MD, October 1971. Prepared for NASA/GSFC.

[3] F. Crawley, George L. Server, and David G. Mohr. Experimental measurements of passive material and structural damping for flexible space structures. *Acta Astronautica*, 10(5-6):381–393, 1983. Reprinted in *Vibration Damping 1984 Workshop Proceedings*, pages A23 to A35, edited by Lynn Rogers, Flight Dynamics Laboratory, Air Force Wright Aeronautical Laboratories, Wright-Paterson Air Force Base, Ohio 45433.

[4] Neal Granick and Jesse E. Stern. *Material Damping of Aluminum by a Resonant-Dwell Technique.* Technical Report NASA TN D-2893, NASA, Washington, DC, 1965.

[5] Cyril M. Harris and Charles E. Crede, editors. *Shock and Vibration Handbook*, chapter 37, pages (37)1–(37)34. Volume 2, McGraw-Hill Book Company, New York, 1961.

[6] D. L. Jensen. Structural damping of shuttle orbiter and ascent vehicles. In Lynn Rogers, editor, *Vibration Damping 1984 Workshop Proceedings*, pages Z2–Z14, Flight Dynamics Laboratory, Air Force Wright Aeronautical Laboratories, Wright-Paterson Air Force Base, Ohio 45433, 1984.

[7] John William Strutt, 3^{d} Baron Rayleigh. *The Theory Of Sound.* Dover Publications, New York, First American edition, 1945. First edition: London, Vol. 1 in 1877 and Vol. 2 in 1878; Second edition: London, Vol. 1 in 1894 and Vol. 2 in 1896.

[8] James W. Mar. Some musings on how to make damping a creative force in design. In Lynn Rogers, editor, *Vibration Damping 1984 Workshop Proceedings*, pages A2–A7, Flight Dynamics Laboratory, Air Force Wright Aeronautical Laboratories, Wright-Paterson Air Force Base, Ohio 45433, 1984.

[9] D. McDanels. Analysis of stress-strain, fracture, and ductility behavior of aluminum matrix composites containing discontinuous silicon carbide reinforcement. *Metallurgical Transactions A*, 16A:1105–1115, 1985.

[10] R. D. Mindlin and H. Deresiewicz. Timoshenko's shear coefficient for flexural vibrations of beams. In *Proceedings of the Second U. S. National Congress of Applied Mechanics*, pages 175–178, The American Society of Mechanical Engineers, 1955. Reprinted in **Vibration: Beams, Plates, and Shells**, edited by Arturs Kalnins and Clive L. Dym, Dowden, Hutchinson & Ross, Inc., Stroudsburg, PA, 1976.

[11] Gerald Pickett. Equations for computing elastic constants from flexural and torsional resonant frequencies of vibration of prisms and cylinders. Proceedings, *Am. Soc. Testing Materials*, 45:846–865, 1945.

[12] M. Sambasiva Rao, P. S. Nair, and S. Durvasula. Equivalent dynamic models for a spacecraft and its subsystems. *ESA Journal*, 10(1):93–111, 1986.

[13] J. Schoutens. Simple and precise measurements of fibre volume and void fractions in metal matrix composite materials. *Journal Of Materials Science*, 19:957–964, 1984.

[14] Jacques E. Schoutens. *Discontinuous Silicon Carbide Reinforced Aluminum Metal Matrix Composites Data Review.* MMCIAC Databook Series MMCIAC No. 000461, DOD Metal Matrix Composites Information Analysis Center, 816 State Street, PO Drawer QQ, Santa Barbara, CA 93102, December 1984.

[15] S. Spinner, T. W. Reichard, and W. E. Tefft. A comparison of experimental and theoretical relations between Young's modulus and the flexural and longitudinal resonance frequencies of uniform bars. *Journal of Research of the National Bureau of Standards*, 64A(2):147–155, 1960.

[16] Sam Spinner and Wayne E. Tefft. A method for determining mechanical resonance frequencies and for calculating elastic moduli from these frequencies. Proceedings, *American Society for Testing and Materials*, 61:1221–1238, 1961.

[17] Sam Spinner and Rudolph C. Valore, Jr. Comparison of theoretical and empirical relations between the shear modulus and torsional resonance frequencies for bars of rectangular cross section. *Journal of Research of the National Bureau of Standards*, 60(5):459–464, 1958.

[18] J. Sudey, Jr. and J. R. Schulman. In orbit measurements of Landsat-4 Thematic Mapper dynamic disturbances. In 35^{th} *Congress of the International Astronautical Federation*, American Institute of Aeronautics and Astronautics, 1633 Broadway, New York, NY 10019, 1984. IAF-84-117.

[19] Wayne E. Tefft and Sam Spinner. Cross-sectional correction for computing Young's modulus from longitudinal resonance vibrations of square and cylindrical rods. *Journal of Research of the National Bureau of Standards*, 66A(2):193–197, 1962.

[20] Nancy S. Timmerman and John Doherty. *Loss Factors Measured in Metal Matrix Composite Materials.* Final Report on "Contract No. DAAG46-82-C-0060" AMMRC TR 84-22, Bolt Beranek and Newman Inc., 10 Moulton Street, Cambridge, MA 02138, June 1984. Prepared for the Army Materials and Mechanics Research Center. Approved for public release; distribution unlimited.

[21] Stephen P. Timoshenko. LXVI. On the correction for shear of the differential equation for transverse vibrations of prismatic bars. *Philosophical Magazine, Series 6*, 41:744–746, 1921. Reprinted in **Vibration: Beams, Plates, and Shells**, edited by Arturs Kalnins and Clive L. Dym, Dowden, Hutchinson & Ross, Inc., Stroudsburg, PA, 1976.

[22] Stephen P. Timoshenko, D. H. Young, and W. Weaver, Jr. *Vibration Problems in Engineering.* John Wiley & Sons, New York, third edition, 1955.

[23] Y. S. Touloukian, R. K. Kirby, R. E. Taylor, and P. D. Desai. *Thermophysical Properties of Matter.* IFI/Plenum, New York and Washington, 1973.

[24] Graeme G. Wren and Vikram K. Kinra. An experimental technique for determining a measure of structural damping. *Journal of Testing and Evaluation*, 16(1):77–85, 1988.

[25] Clarence Zener. *Elasticity and Anelasticity of Metals.* The University of Chicago Press, Chicago, Illinois, 1948.

REPORT DOCUMENTATION PAGE

Form Approved
OMB No. 0704-0188

1. AGENCY USE ONLY *(Leave blank)*	2. REPORT DATE	3. REPORT TYPE AND DATES COVERED
	March 1996	Technical Memorandum

4. TITLE AND SUBTITLE
Elastic Moduli and Damping of Vibrational Modes of Aluminum/Silicon Carbide Composite Beams

5. FUNDING NUMBERS
Code 313

6. AUTHOR(S)
Henning Leidecker

7. PERFORMING ORGANIZATION NAME(S) AND ADDRESS (ES)
Goddard Space Flight Center
Greenbelt, MD 20771

8. PEFORMING ORGANIZATION REPORT NUMBER
96B00026

9. SPONSORING / MONITORING AGENCY NAME(S) AND ADDRESS (ES)
National Aeronautics and Space Administration
Washington, DC 20546-0001

10. SPONSORING / MONITORING AGENCY REPORT NUMBER
NASA TM-104626

11. SUPPLEMENTARY NOTES

12a. DISTRIBUTION / AVAILABILITY STATEMENT
Unclassified - Unlimited
Subject Category 24

Availability: NASA CASI (301) 621-0390.

12b. DISTRIBUTION CODE

13. ABSTRACT *(Maximum 200 words)*

Elastic and shear moduli were determined for two aluminum matrix composites containing 20 and 40 volume percent discontinuous silicon carbide, respectively, using transverse, longitudinal, and torsional vibrational modes of specimens prepared as thin beams. These moduli are consistent with those determined from stress-strain measurements. The damping factors for these modes were also determined. Thermal properties are used to show that part of the damping of transverse modes is caused by the transverse thermal currents discussed by C. Zener (*thermo-elastic damping*); this damping is frequency-dependent with a maximum damping factor of ~ 0.002. The remaining damping is frequency-independent, and has roughly similar values in transverse, longitudinal, and torsional modes: ~0.0001.

14. SUBJECT TERMS
Damping, Aluminum Silicon carbide, vibration spectrum.

15. NUMBER OF PAGES
56

16. PRICE CODE

17. SECURITY CLASSIFICATION OF REPORT	18. SECURITY CLASSIFICATION OF THIS PAGE	19. SECURITY CLASSIFICATION OF ABSTRACT	20. LIMITATION OF ABSTRACT
Unclassified	Unclassified	Unclassified	UL

National Aeronautics and
Space Administration
Goddard Space Flight Center
Greenbelt, Maryland 20771

SPECIAL FOURTH-CLASS RATE
POSTAGE & FEES PAID
NASA
PERMIT No. G27